

Antireflective Multilayer Surface with Self-Cleaning Subwavelength Structures

Juan Rombaut,* Sofia Martínez, Umberto Maria Matera, Prantik Mazumder, and Valerio Pruneri*

Cite This: *ACS Photonics* 2021, 8, 894–900

Read Online

ACCESS |



Metrics & More



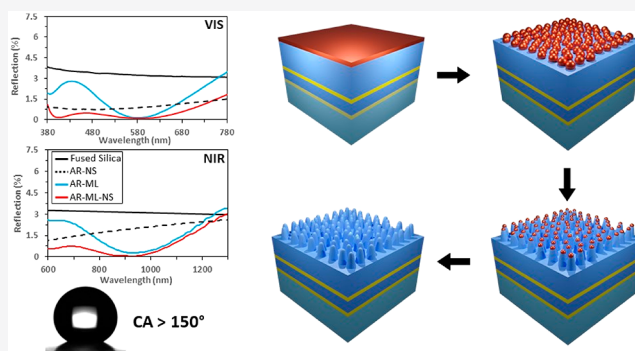
Article Recommendations



Supporting Information

ABSTRACT: The suppression of optical reflection from a surface is essential in many applications, ranging from displays with reduced disturbance from ambient light to high-efficiency photovoltaic cells and stable light detection and ranging (LIDAR) systems. Traditionally, antireflection (AR) surfaces are made of multilayer (ML) coatings that produce destructive interference of light beams reflected from each interface. More advanced AR surfaces are based on biomimetic nanostructures (NS) that rely on a gradation of refractive index to suppress reflection. While AR-ML coatings tend to work for restricted light wavelengths and angles of incidence, AR-NS can be broadband and omnidirectional. In addition, AR-NS can provide superhydrophobicity and self-cleaning effects. Unfortunately, AR-NS often suffer from mechanical failure, this being more critical for taller structures required for operation at longer wavelengths. Here we propose to combine ML and shorter NS to achieve an AR surface with several crucial advantages, including greater spectral and angular bandwidth and water repellency compared to only AR-ML, easier fabrication, lower scattering, and higher mechanical durability compared to only AR-NS, which requires taller structures. We present theoretical and experimental studies for combined AR-ML-NS glass surfaces operating in the visible (VIS) between 380 and 780 nm and especially at longer wavelengths in the near-infrared (NIR) at around 900 nm, where applications such as LIDAR for autonomous vehicles are of high interest.

KEYWORDS: antireflective, self-cleaning, biomimetics, multilayer coating, nanostructures



Antireflection (AR) surfaces are essential elements in many applications. For example, in lasers they enable loss reduction of intracavity elements, in LIDAR they increase signal stability, in display screens they reduce dazzling effects of environmental light, and in photovoltaic cells they increase the light intensity reaching the active layers.^{1–3} Besides AR, superhydrophobicity is another attribute that is often desired, as it promotes self-cleaning behavior^{4–6} in outdoor applications. It is thus technologically relevant to search for AR and superhydrophobic surfaces capable of meeting optical and mechanical durability requirements optimized for specific applications.⁷

Commercially available AR solutions are usually made of single-layer or multilayer (AR-ML) coatings.^{8–15} These are built on a stack of thin layers of different refractive indices, which reduces the overall reflection due to the destructive interference of the multiple wavefronts reflected at each interface. By tuning the number, thicknesses, and the optical properties (or choice of materials), it is possible to optimize the AR-ML for specific spectral regions. Due to the resonance nature of the interference, the response tends to be narrowband in wavelength and angle of incidence. Use of varying thicknesses (i.e., chirped) or graded index ML

structure may extend the AR bandwidth but at the expense of the minimum reflectivity achievable.¹⁶

Another AR approach for transparent surfaces inspired by nature is the biomimetic moth eye that is based on artificially created nanostructures (NS).^{17–29} The AR effect originates from a smooth refractive index gradient at the interface between air and the surface. It is possible to achieve higher spectral and angular broadband properties in AR-NS than in AR-ML, yet maintaining negligible scattering loss due to the subwavelength dimensions of the NS.^{26–30} On the other hand, NS are also found on many natural surfaces, such as lotus leaf, which show a certain degree of self-cleanliness due to superhydrophobicity that is characterized by a high stationary contact angle and a low hysteresis or sliding angle.^{30–38} By coating the artificially fabricated NS with low surface energy molecules, such as a self-assembled monolayer (SAM) of a

Received: December 16, 2020

Published: February 17, 2021

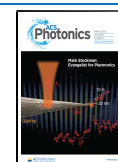
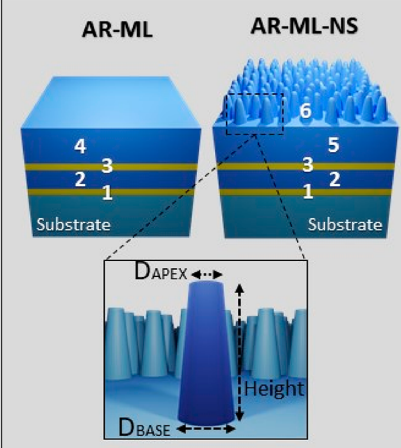


Table 1. Antireflection Multilayer (AR-ML) and AR-ML with Nanostructures (AR-ML-NS)^a


ML layer	Material	Thickness (VIS)	Thickness (NIR)		
Substrate	Fused Silica	-	-		
1	TiO ₂	10.0 nm	16.3 nm		
2	SiO ₂	47.5 nm	77.7 nm		
3	TiO ₂	15.0 nm	24.5 nm		
4	SiO ₂	107.5 nm	175.9 nm		
5	SiO ₂	100.0 nm	150.0 nm		
NS	Material	Height	D _{BASE}	D _{APEX}	Density
6	SiO ₂	150nm	60nm	50nm	50 particles/μm ²

^aAs a prototypical AR-ML-NS example, we study ML composed of five alternating layers of SiO₂ and TiO₂ on fused silica substrate with NS made of nanopillars on the top layer. Geometrical parameters for structures for visible (VIS) and near infrared (NIR) operations, between 380 and 780 nm and at around 900 nm, respectively, are given. The AR-ML structure consisting of four alternating layers is also prototypical and provides benchmarking for comparing optical performance (Figure 1).

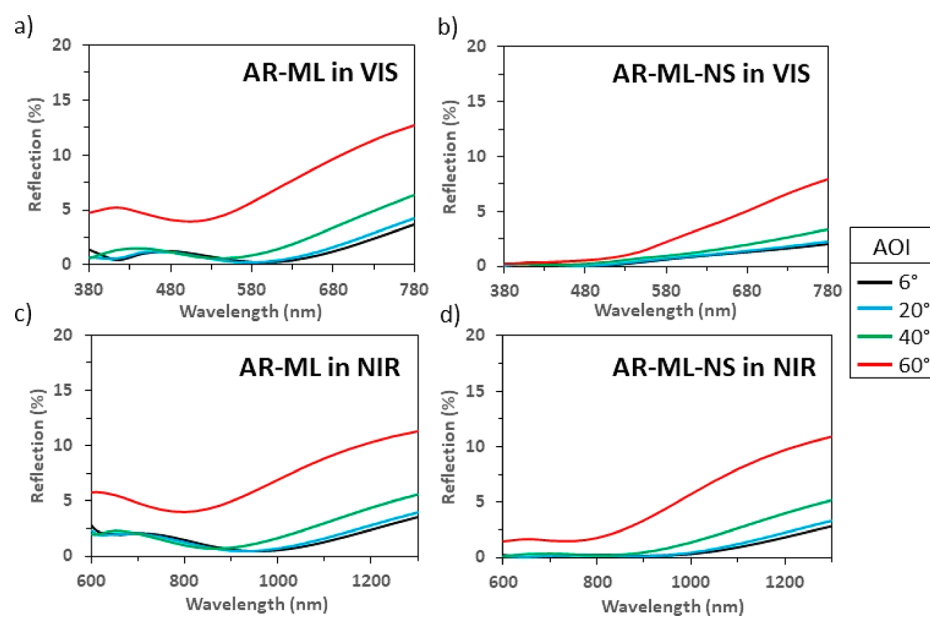


Figure 1. Simulated comparison of antireflection (AR) effect between multilayer coating, without (AR-ML) and with (AR-ML-NS) nanopillars, as a function of angle of incidence (AOI): (a, b) visible (VIS) and (c, d) near-infrared (NIR). All simulations refer to only one substrate surface, that is, the back surface is placed at an infinite distance as if it had zero reflectivity. Refractive index coefficients used in the simulations are shown in Supporting Information, Figure S3.

fluoropolymer, a large contact and small sliding angle for water can be obtained. That is, surfaces can be artificially engineered through physical nanostructuring and chemical functionalization to achieve superhydrophobicity (SH) and self-cleaning properties.

Thus, NS can provide both broadband AR and SH. However, in practice, such structures are not always easy to make with scalable techniques and usually suffer from poor mechanical durability. These limitations become even more daunting at higher operating wavelengths. On the one hand, the height of the nanostructures need to increase to maintain the AR properties at longer wavelengths, which makes the aspect ratio (height/diameter) higher that, in turn, renders them more vulnerable to mechanical damage,²⁵ more

scattering, and difficulty in fabrication. On the other hand, while AR-ML can provide more durable surfaces due to their planar structures, their AR is narrowband and their wetting property cannot achieve superhydrophobicity in the absence of surface textures.

In this paper we propose a new AR-ML-NS design combining AR-ML with shallow NS on the top layer, which provides the following advantages: (i) greater spectral and angular bandwidth and water repellency compared to AR-ML and (ii) easier fabrication, lower scattering, and higher mechanical durability compared to AR-NS due to shallower structures. We present theoretical and experimental studies for combined AR-ML-NS glass surfaces operating in the visible (VIS) between 380 and 780 nm and especially at longer

wavelengths in the near-infrared (NIR) at 900 nm, where applications such as LIDAR for autonomous vehicles are of high interest.

RESULTS AND DISCUSSION

In these preliminary studies, we used four ML layers to demonstrate the AR-ML-NS principle and for the ease of fabrication (see sketch in Table 1). However, the concept applies to any different number of ML layers, different choice of materials, and NS geometry, which may lead to more optimal results. We first simulated the structure, then fabricated it, and finally measured its optical response. The NS and ML are made of nanopillars and alternating layers of SiO₂ and TiO₂, respectively. In Table 1, we also show the AR-ML structure used for comparison and indicate the geometrical parameters of the ML and NS for operation either in the VIS or NIR. The ML was designed and optimized using full-wave electromagnetic simulations and a commercial finite element package (COMSOL Multiphysics Modeling Software) for both ML without (AR-ML) and with nanopillars (AR-ML-NS). The NS geometry was optimized to obtain a minimum reflection considering the fabrication constraint, that is, the typical nanopillar density (50 nanopillars per micron square) and base diameter (60 nm). Parametric simulations indicate that a height and apex diameter of about 150 and 50 nm, respectively, provide close to optimal operation (Supporting Information, Figure S1). These dimensions are confirmed for the fabricated NS by scanning electron microscopy (SEM) images, see Supporting Information, Figure S2.

Figure 1 shows the simulated reflection for unpolarized light as a function of wavelength for the VIS (a, b) and NIR (c, d) regions and different angle of incidence (AOI). The NS of the top layer improves the angular behavior on the AR-ML surface, that is, it provides flatter and lower reflectivity over a larger wavelength range and angle of incidence (AOI). Note that, as expected, the effect of the NS on the AR-ML is larger in the VIS range. Taller structures would lead to a comparable benefit in the NIR range, but could lead to mechanical durability issues, as it will be clear in the following sections of the paper.

Two sets of samples were fabricated to experimentally investigate the effect of the NS on an AR-ML in the VIS and NIR region. The four-layer ML coating with a geometry defined in Table 1 was deposited by sputtering on a fused silica substrate (see Methods for fabrication details). Subsequently, the top layer was nanostructured following the fabrication process shown in Figure 2 and described in previous publications.^{27,29,39} First, an ultrathin copper film was deposited by sputtering, then it was thermally dewetted to form particles that were used as a mask for the subsequent reactive ion etching. After removal of the residual copper, the nanopillars were formed, with geometrical parameters listed in Table 1 and also used for simulations of Figure 1. Note that the nanopillar dimensions must be a subwavelength to avoid scattering, and their height, we chose 150 nm, was a compromise between adequate SH and mechanical durability. Also, the initial thickness of the last layer of the AR-ML-NS was larger than that of the final AR-ML structure to take into account the subsequent NS.

Both the AR-ML and AR-ML-NS samples were optically characterized by measuring their transmission and reflection, which are shown in Figure 3 along with the bare fused silica substrate. Figures 3a,b also contains results on AR-NS (same nanostructure design as for AR-ML-NS), which has nano-

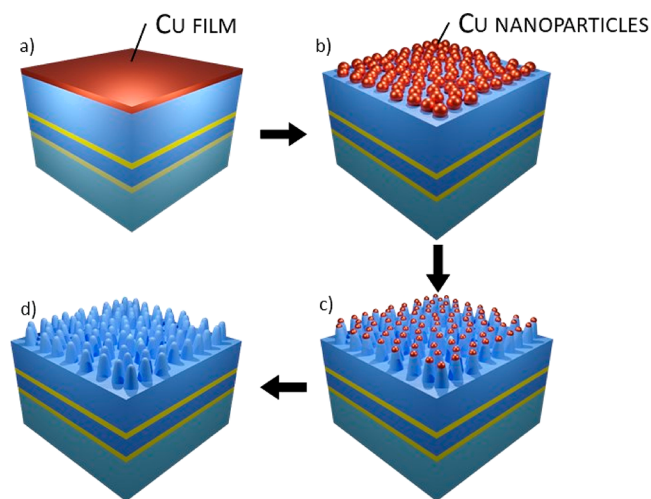


Figure 2. Fabrication of nanostructures (NS) on top of multilayer (ML) coating. Ultrathin copper (Cu) film is deposited by sputtering (a) and thermally dewetted into nanoparticles (b). The metal nanoparticles are then used as an etching mask to create nanopillars in the last ML layer by reactive ion etching (c). The residual Cu mask is finally chemically removed (d).

pillars with similar dimensions as those of the AR-ML-NS. Note that the AR-NS structures should be deeper for optimum AR response. The AR-ML structure clearly shows an AR effect, that is, lower reflection and higher transmission, with respect to the bare substrate. The combined AR-ML-NS structure for both VIS and NIR ranges presents a flatter AR response with lower reflectivity and higher transmission than those of the AR-ML counterpart. As expected, this is more evident for the VIS range considering that the NS height is the same for both VIS and NIR while the wavelength nearly doubles. The performance of the AR-ML-NS is also significantly superior to AR-NS with the same nanopillar structure, especially in the NIR range. The angular dependence of both AR-ML and AR-ML-NS structures is presented in Figure 3 and confirms the expected results from simulations represented in Figure 1.

Another important yet often neglected parameter for optical surfaces is the scattering, which can be quantified by the haze parameter, that is, the percentage of incident light diffused by the sample at an angle larger than 2.5°. It is known that NS, if not subwavelength, can cause significant scattering. In our case, we measured haze values of 0.03% and 0.13% for the AR-ML and AR-ML-NS surfaces, respectively, indicating very low scattering. To obtain a similar AR effect with only NS, higher nanopillars are needed and, as a result, the haze values would have been higher. Haze is measured in the VIS range where our instrument operates. For the NIR, given that the NS geometry is similar and the wavelength much larger, the haze value and scattering for the combined AR-ML-NS surface should be even lower.

The self-cleaning capabilities are related to the wetting properties between a water droplet and the surface. Static contact angles (CA), sliding angle, and contact angle hysteresis (CAH) before and after the application of a low surface tension fluorosilane were measured (Figure 4). After fabrication, the AR-ML exhibited hydrophilic behavior (CA < 90°), while AR-ML-NS was superhydrophilic (CA < 10°). After functionalizing with fluorosilane, the AR-ML became hydrophobic (CA = 115°) while AR-ML-NS reached SH state (CA > 150°) with low sliding angle (~6°) and low CA

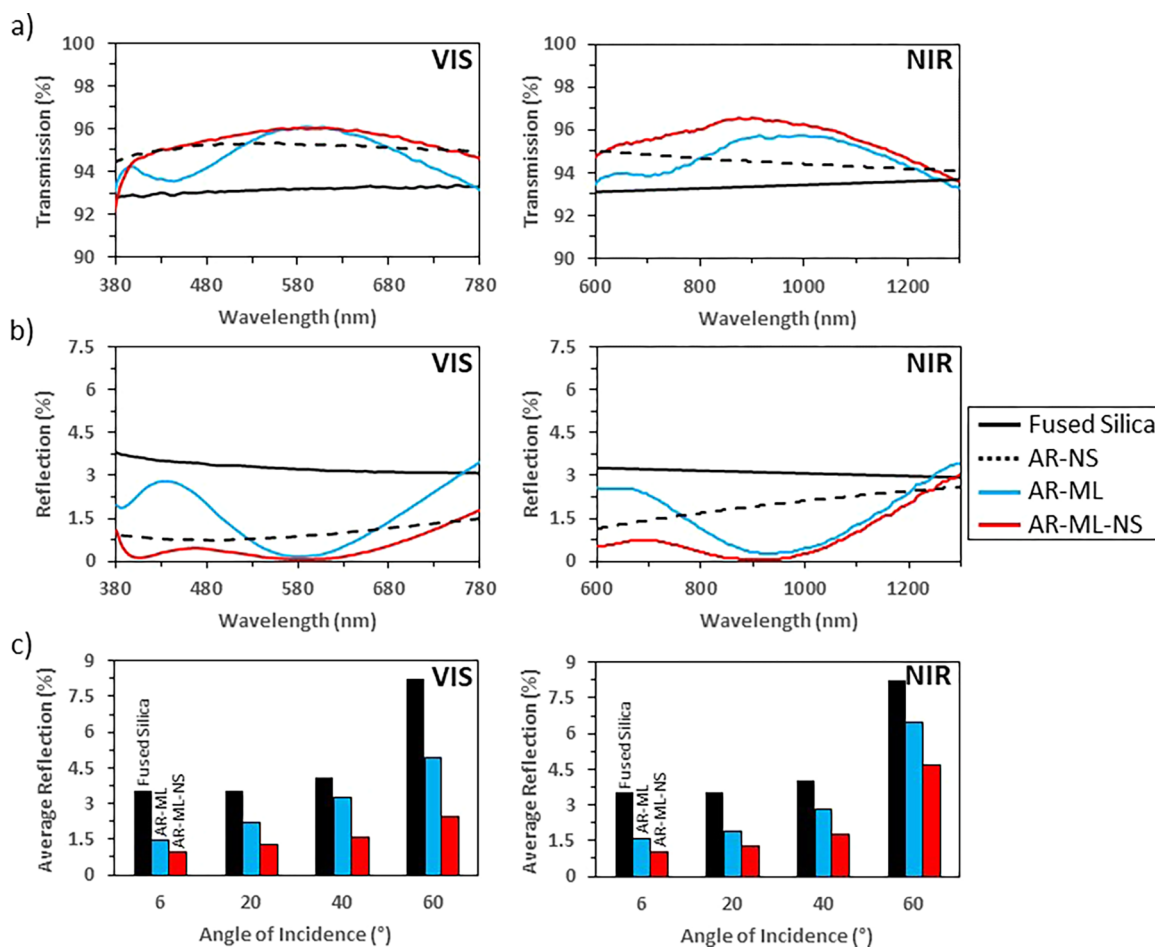


Figure 3. Experimental comparison: total two-side transmission (a) and one-side reflection (b) at close to normal incidence (angle of incidence 6°) between antireflective nanostructured fused silica (AR-NS), antireflective multilayer (AR-ML), and antireflective multilayer with nanostructures (AR-ML-NS; 150 nm height nanopillar) optimized for the visible (VIS) region ($\lambda = 550$ nm; left) and the near-infrared (NIR) region ($\lambda = 900$ nm; right). Experimental one-side reflection, averaged values over VIS and NIR range, of the proposed AR-ML and AR-ML-NS structures for different angles of incidence. For comparison, we also show the calculated bare fused silica substrate (c). In addition to providing superhydrophobicity and self-cleaning, the NS reduces reflection and thus increases transmission (flat response) over a large wavelength range and for different angles of incidence.

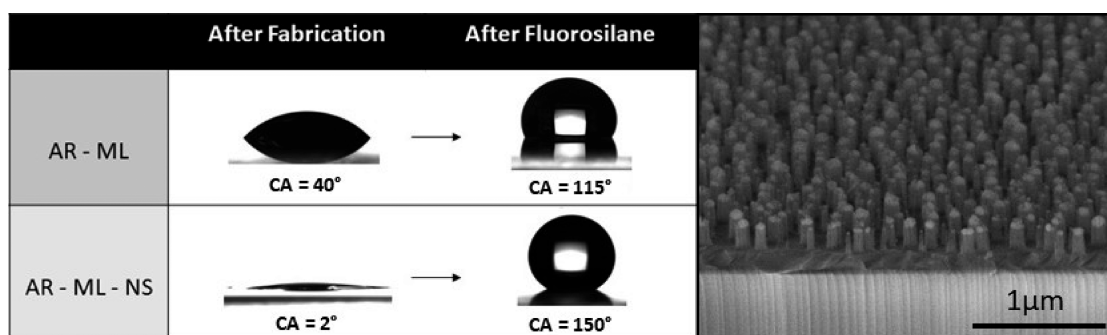


Figure 4. Wetting characterization. Comparison of antireflection multilayer surfaces flat ((AR-ML) and nanostructured (AR-ML-NS) before and after the application of the fluorosilane self-assembly monolayer (SAM). SEM image of the AR-ML-NS top layer

hysteresis ($CA_H < 8^\circ$), which indicates a strong roll-off effect. The results thus confirm that our initial design, that is, 150 nm nanopillars, is sufficient to achieve SH without requiring taller structures.

The AR-ML-NS samples were also tested for mechanical durability using a crockmeter (Figure 5). A common commercially available “eye glass” cleaning cloth was used under standard conditions (pressure of 4.5 N/cm 2). After 50

passes, the SEM analysis revealed that the structure was preserved. This was also consistent with optical transmission measurements before and after crockmeter (Figure 5c) and with calculations showing that maximum tension is well below the breaking point of silica.²⁵ If much taller NS are created, for example, 400 nm instead of 150 nm, these do not pass such a mechanical test (Supporting Information, Figure S4). A height of 400 nm would be required for an AR-NS (without ML)

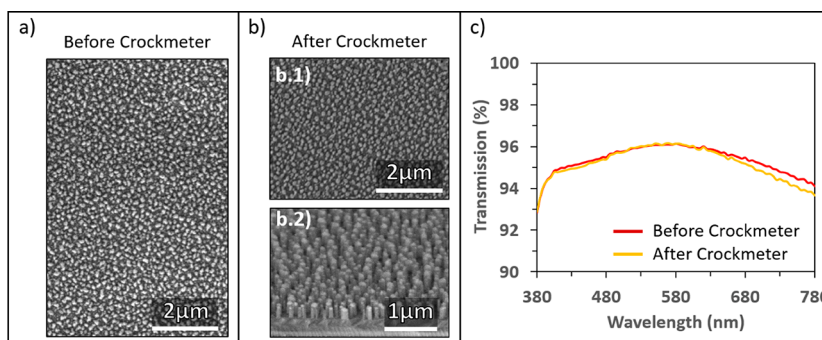


Figure 5. Mechanical durability of the antireflective multilayer nanostructured (AR-ML-NS) surface tested by crockmeter. SEM image comparison between before (a) and after (b) more than 50 passes performed with standard 4.5 N/cm^2 pressure using an eyeglass cleaning cloth. Top view (a and b.1) and cross section (b.2). The fact that the sample passes the test is also confirmed by optical transmission measurements (c).

operating in the NIR at around 900 nm. This makes evident the benefit of the proposed concept, to combine NS and ML, to achieve AR, SH, and mechanical resistance at the same time.

METHODS

Characterization of Multilayer (ML) Materials. The ML designs are based on intercalated TiO_2 and SiO_2 thin films deposited by a magnetron sputtering system (ATC Orion 8m, AJA Internacional, Inc.). The TiO_2 and SiO_2 material targets are from Kurt J. Lesker Company.

Before the fabrication, characterization of the composing materials was performed for measuring parameters essential for the simulations and designs. First, the deposition rate was characterized on Si/SiO_2 substrates with multiple depositions and thickness measurements with an atomic force microscopy system (Veeco Dimension 3100, Bruker) and a profilometer (KLA Tencor). Once the thickness of the different layers was characterized, a spectroscopic ellipsometry study (SOPRA, GESS) was performed with a 75 W xenon lamp source to obtain the refractive index and absorption coefficient of both TiO_2 and SiO_2 (Supporting Information, Figure S3).

Modeling of Optical Response. In order to calculate the optimum thicknesses of the ML layers, a commercially available software (COMSOL Multiphysics) was used. The ML structures were simulated using periodic boundary conditions. The AR-ML was modeled as a square cell, whereas the AR-ML-NS was modeled as a square cell with a centered pillar. The geometry of the pillar was extracted after a statistical analysis from SEM images. Different parametric sweeps were run to optimize the layers thicknesses of the AR-ML for the VIS and NIR. Subsequently, considering a fixed size of the nanopillars (150 nm height) and conical shape (Supporting Information, Figure S1), the last layer of the ML thickness was chosen to optimize the AR performance for the AR-ML-NS.

Fabrication of Antireflective Multilayer (AR-ML) Coating. Double-sided, optically polished, ultraviolet-grade fused silica (FS) glass, with a thickness of 1 mm and an area of 1 in. square, were used as substrates. The surfaces were cleaned in acetone followed by ethanol in an ultrasonic bath for 10 min each. The substrates were then rinsed in deionized water and dried with nitrogen, followed by oxygen plasma cleaning (PVA TePla 300 SemiAuto Plasma Asher) for 10 min with 300 mL/min of O_2 and 700 W of power. For the SiO_2 layers, the sputtering deposition was performed at a base pressure of 10^{-8} Torr, room temperature, 175 W of RF power, 20 standard cubic centimeters per minute (sccm) of pure argon (Ar), and 2 sccm of oxygen to maintain the stoichiometry of the target

material deposited on the substrate. The working pressure was 1.5×10^{-3} Torr, the deposition rate was 0.012 nm/s and the target–substrate distance was 35 cm. For the TiO_2 layers, the deposition was performed at a base pressure of 10^{-8} Torr, room temperature, 175 W of RF power, 20 sccm of pure Ar, and 0.4 sccm of oxygen to maintain the stoichiometry of the target material deposited on the substrates. The working pressure was 1.5×10^{-3} Torr, the deposition rate was 0.018 nm/s, and the target–substrate distance was 35 cm. By varying the time of deposition, it is possible to adjust the thickness of each layer according to the desired design.

Antireflective Multilayer with Nanostructures (AR-ML-NS) Coating. The AR-ML samples were cleaned in acetone, followed by ethanol, in an ultrasonic bath for 10 min each. Afterward, they were rinsed in deionized water and dried with nitrogen, followed by oxygen plasma cleaning for 10 min with 300 mL/min of O_2 and 700 W of power. Using the same sputtering process as for the multilayer fabrication, additional SiO_2 was deposited to increase the thickness of the last layer prior to the nanostructuring process. If the last layer of the AR-ML was directly nanostructured, the destructive interference phenomenon would change, reducing the AR effect. Depending on the structure, the last layer has to be modified prior to nanostructuring in order to obtain optimal optical results. The optimal thickness of layer #5 for the VIS and NIR structures was extracted from a parametric simulation and is shown in Table 1. An ultrathin film of copper (Cu) with a thickness of 6 nm was deposited by sputtering on top of the multilayer. The deposition was performed at a base pressure of 10^{-8} Torr, room temperature, 100 W of DC power, and 25 sccm of pure Ar. The working pressure was 1.5×10^{-3} Torr, the deposition rate was 0.166 nm/s, and the target–substrate distance was 40 cm. In order to create the nanostructure, the samples were subjected to a rapid thermal annealing process (RTA). Dewetting takes place due to minimization of the surface free energy of the system,⁴⁰ and the metal film reduces its surface area by self-collecting into small islands. Before RTA, the samples were blown with a N_2 gun to ensure that the surface was completely clear of small dust particles and pollutants that could alter the dewetting process. The RTA was carried out in the Tsunami™ RTP-600S system at a temperature of 600 °C for 450 s. It is possible to tune the density and size of the nanoparticles by adjusting the Cu initial film, the temperature and the time of the RTA process. The nanoparticles created by dewetting were used as an etching mask. Dry etching of the samples was performed by Plasmalab System 100 (Oxford Instruments) with 300 W of RF power

(850 DCV) at 10 mTorr in 40 sccm Ar/5 sccm CHF₃ plasma. The etching time determines the pillar heights. Afterward, the residual mask of Cu was chemically removed with ammonium persulfate.

Hydrophobic Fluorosilane Coating. The surface free energy of the samples was modified by applying a fluorosilane SAM coating. The fluorosilane used for this experiment was OPTOOL UF503 (Daikin) dissolved in NOVEC 7200 (3M) with a proportion of 1:1000. The mixture was stirred for 15 min before its use. The substrates were pretreated with O₂ plasma with a plasma cleaner system (PVA TePla 300 SemiAuto Plasma Asher) in order to functionalize the surface and remove defects and pollutants. The samples were dip-coated for 3 min and then cured at 50° for 2 h in a convection oven. Finally, in order to remove the excess layers of the fluorosilane, the samples were ultrasonically cleaned in a NOVEC 7200 bath for 2 min.

Optical, Morphological, and Wetting Characterization. The optical transmission and reflection were measured in the wavelength ranges of 380–780 nm for VIS and from 600 to 1300 nm for NIR by using a UV–vis–NIR spectrophotometer (PerkinElmer Lambda 950). Reflection measurements at normal incidence in Figure 3 were carried out with an AOI of 6°. The experimental values of one-side reflection in Figure 3 were calculated from the two-side reflection following ref. 29, considering that the back surface is flat. For Figure 3b, the two-side reflection was directly measured. Our set-up only allowed us to measure the angular dependent two-side transmission (T) but not reflection (R). For figure 3c we thus calculated two-side R from measured T using the formula $R \approx 100\% - T$, as scattering (haze) is very low.²⁹ Figure 3c. Scattering was characterized by measuring the haze using a Haze-meter (BYK-Gardner 4601 haze-gloss). Multiple measurements were carried out to obtain the average values given in the paper. The morphology of the surface was examined by a scanning electron microscope (FEG-SEM, Inspect F, FEI Systems) working from 2 to 5 kV accelerating voltage at 10 mm distance. The wetting properties of the samples were determined with a drop shape analysis system (DSA-100, Krüss GmbH) by measuring the static and dynamic water CA. Different areas of each sample were examined and averaged.

Mechanical Resistance Test. The durability of the proposed structure was studied using a crockmeter machine (M238BB Electronic Crockmeter, SDL ATLAS). The test follows the standards of the American Association of Textile Chemists and Colorists (AATCC) as test method 8, with a constant force of 9 N over a 2 cm² surface.

CONCLUSIONS

In this paper, we propose a multifunctional antireflective and superhydrophobic optical surface (AR-ML-NS) that combines two AR technologies: ML coatings and subwavelength biomimetic NS. We have experimentally demonstrated that the combined structure can provide optimal AR properties, with low reflectivity, broadband wavelength operation, and improved angular response while having also self-cleaning properties reaching superhydrophobicity. The fabrication process uses scalable methods with lithography-free techniques that can be implemented for different materials and surfaces. The structure can be designed for different wavelength ranges, even in the infrared region, while keeping good mechanical resistance and adding superhydrophobicity. All these features

make the developed structure very effective and versatile to be implemented in different devices or applications.

ASSOCIATED CONTENT

Supporting Information

The Supporting Information is available free of charge at <https://pubs.acs.org/doi/10.1021/acsp Photonics.0c01909>.

Figure S1 presents a parametric simulation to study the effect of the NS geometry on the average reflection of the AR-ML-NS structure. Figure S2 shows a SEM image for statistical analysis and the 3D model design to study and optimize the proposed structure with simulations. In Figure S3, results from the ellipsometry study with the refractive index of the materials used in the ML coating are presented. Figure S4 shows the mechanical resistance comparison between two samples with different pillar heights (PDF)

AUTHOR INFORMATION

Corresponding Authors

Valerio Pruneri – ICFO – Institut de Ciències Fotòniques, The Barcelona Institute of Science and Technology, 08860 Castelldefels (Barcelona), Spain; ICREA – Institució Catalana de Recerca i Estudis Avançats, 08010 Barcelona, Spain; Email: valerio.pruneri@icfo.eu

Juan Rombaut – ICFO – Institut de Ciències Fotòniques, The Barcelona Institute of Science and Technology, 08860 Castelldefels (Barcelona), Spain; orcid.org/0000-0002-6438-0765; Email: juan.rombaut@icfo.eu

Authors

Sofia Martínez – ICFO – Institut de Ciències Fotòniques, The Barcelona Institute of Science and Technology, 08860 Castelldefels (Barcelona), Spain

Umberto Maria Matera – ICFO – Institut de Ciències Fotòniques, The Barcelona Institute of Science and Technology, 08860 Castelldefels (Barcelona), Spain

Prantik Mazumder – Corning Research and Development Corporation, Corning, New York 14831, United States

Complete contact information is available at: <https://pubs.acs.org/doi/10.1021/acsp Photonics.0c01909>

Author Contributions

The manuscript was written through contributions of all authors. All authors have given approval to the final version of the manuscript.

Notes

The authors declare no competing financial interest.

ACKNOWLEDGMENTS

Author acknowledges financial support from the Spanish State Research Agency through the “Severo Ochoa” Programme for Centres of Excellence in R&D (CEX2019-000910-S) and Project TUNA-SURF (PID2019-106892RB-I00), Fundació Cellex, Fundació Mir-Puig, and from Generalitat de Catalunya through the CERCA Program, from AGAUR 2017 SGR1634.

REFERENCES

(1) Cai, J.; Qi, L. Recent Advances in Antireflective Surfaces Based on Nanostructure Arrays. *Mater. Horiz.* **2015**, *2* (1), 37–53.

- (2) Han, Z. W.; Wang, Z.; Feng, X. M.; Li, B.; Mu, Z. Z.; Zhang, J. Q.; Niu, S. C.; Ren, L. Q. Antireflective surface inspired from biology: A review. *Biosurface and Biotribology* **2016**, *2* (4), 137–150.
- (3) Buskens, P.; Burghoorn, M.; Mourad, M. C. D.; Vroon, Z. Antireflective Coatings for Glass and Transparent Polymers. *Langmuir* **2016**, *32* (27), 6781–6793.
- (4) Bhushan, B.; Jung, Y. C. Natural and Biomimetic Artificial Surfaces for Superhydrophobicity, Self-Cleaning, Low Adhesion, and Drag Reduction. *Prog. Mater. Sci.* **2011**, *56* (1), 1–108.
- (5) Nishimoto, S.; Bhushan, B. Bioinspired Self-Cleaning Surfaces with Superhydrophobicity, Superoleophobicity, and Superhydrophilicity. *RSC Adv.* **2013**, *3* (3), 671–690.
- (6) Jeevahan, J.; Chandrasekaran, M.; Joseph, G. B.; Durairaj, R. B.; Mageshwaran, G. Superhydrophobic Surfaces: A Review on Fundamentals, Applications, and Challenges. *J. Coat. Technol. Res.* **2018**, *15* (2), 231–250.
- (7) Scarratt, L. R. J.; Steiner, U.; Neto, C. A Review on the Mechanical and Thermodynamic Robustness of Superhydrophobic Surfaces. *Adv. Colloid Interface Sci.* **2017**, *246* (May), 133–152.
- (8) Rayleigh, J. S. On Reflection of Vibrations. *Proceedings of the London Mathematical Society* **1879**, *s1–11*, 51–56.
- (9) Born, M.; Wolf, E. *Principles Of Optics*, 4th ed.; Pergamon Press: Oxford, 1970, DOI: 10.1039/C4CC01864H.
- (10) Dobrowolski, J. A.; Poitras, D.; Ma, P.; Vakil, H.; Acree, M. Toward Perfect Antireflection Coatings: Numerical Investigation. *Appl. Opt.* **2002**, *41* (16), 3075.
- (11) Raut, H. K.; Ganesh, V. A.; Nair, A. S.; Ramakrishna, S. Antireflective Coatings: A Critical, in-Depth Review. *Energy Environ. Sci.* **2011**, *4* (10), 3779.
- (12) Keshavarz Hedayati, M.; Elbahri, M. Antireflective Coatings: Conventional Stacking Layers and Ultrathin Plasmonic Metasurfaces, A Mini-Review. *Materials* **2016**, *9* (6), 497.
- (13) Khan, S. B.; Wu, H.; Huai, X.; Zou, S.; Liu, Y.; Zhang, Z. Mechanically Robust Antireflective Coatings. *Nano Res.* **2018**, *11* (3), 1699–1713.
- (14) Shimomura, H.; Gemici, Z.; Cohen, R. E.; Rubner, M. F. Layer-by-Layer-Assembled High-Performance Broadband Antireflection Coatings. *ACS Appl. Mater. Interfaces* **2010**, *2* (3), 813–820.
- (15) Garlisi, C.; Trepci, E.; Li, X.; Al Sakkaf, R.; Al-Ali, K.; Nogueira, R. P.; Zheng, L.; Azar, E.; Palmisano, G. Multilayer Thin Film Structures for Multifunctional Glass: Self-Cleaning, Antireflective and Energy-Saving Properties. *Appl. Energy* **2020**, *264* (February), 114697.
- (16) Chhajed, S.; Schubert, M. F.; Kim, J. K.; Schubert, E. F. Nanostructured Multilayer Graded-Index Antireflection Coating for Si Solar Cells with Broadband and Omnidirectional Characteristics. *Appl. Phys. Lett.* **2008**, *93* (25), 251108.
- (17) Wilson, S. J.; Hutley, M. C. The Optical Properties of “Moth Eye” Antireflection Surfaces. *Opt. Acta* **1982**, *29* (7), 993–1009.
- (18) Parker, A. R.; Townley, H. E. Biomimetics of Photonic Nanostructures. *Nat. Nanotechnol.* **2007**, *2*, 347–353.
- (19) Pan, Z.; Cheng, F.; Zhao, B. Bio-Inspired Polymeric Structures with Special Wettability and Their Applications: An Overview. *Polymers* **2017**, *9*, 725.
- (20) Chen, J. Y.; Chang, W. L.; Huang, C. K.; Sun, K. W. Biomimetic Nanostructured Antireflection Coating and Its Application on Crystalline Silicon Solar Cells. *Opt. Express* **2011**, *19*, 14411–14419.
- (21) Oh, S. S.; Choi, C. G.; Kim, Y. S. Fabrication of Micro-Lens Arrays with Moth-Eye Antireflective Nanostructures Using Thermal Imprinting Process. *Microelectron. Eng.* **2010**, *87* (11), 2328–2331.
- (22) Diao, Z.; Hirte, J.; Chen, W.; Spatz, J. P. Inverse Moth Eye Nanostructures with Enhanced Antireflection and Contamination Resistance. *ACS Omega* **2017**, *2* (8), 5012–5018.
- (23) Ji, S.; Song, K.; Nguyen, T. B.; Kim, N.; Lim, H. Optimal Moth Eye Nanostructure Array on Transparent Glass towards Broadband Antireflection. *ACS Appl. Mater. Interfaces* **2013**, *5* (21), 10731–10737.
- (24) Han, G.; Nguyen, T.-B.; Park, S.; Jung, Y.; Lee, J.; Lim, H. Moth-Eye Mimicking Solid Slippery Glass Surface with Icephobicity, Transparency, and Self-Healing. *ACS Nano* **2020**, *14*, 10198.
- (25) Park, K. C.; Choi, H. J.; Chang, C. H.; Cohen, R. E.; McKinley, G. H.; Barbastathis, G. Nanotextured Silica Surfaces with Robust Superhydrophobicity and Omnidirectional Broadband Supertransmissivity. *ACS Nano* **2012**, *6*, 3789–3799.
- (26) Mazumder, P.; Jiang, Y.; Baker, D.; Carrilero, A.; Tulli, D.; Infante, D.; Hunt, A. T.; Pruneri, V. Superomniphobic, Transparent, and Antireflection Surfaces Based on Hierarchical Nanostructures. *Nano Lett.* **2014**, *14*, 4677.
- (27) Tulli, D.; Hart, S. D.; Mazumder, P.; Carrilero, A.; Tian, L.; Koch, K. W.; Yongsunthon, R.; Piech, G. A.; Pruneri, V. *ACS Appl. Mater. Interfaces* **2014**, *6*, 11198–11203.
- (28) Liapis, A. C.; Rahman, A.; Black, C. T. Self-Assembled Nanotextures Impart Broadband Transparency to Glass Windows and Solar Cell Encapsulants. *Appl. Phys. Lett.* **2017**, *111* (18), 183901.
- (29) Infante, D.; Koch, K. W.; Mazumder, P.; Tian, L.; Carrilero, A.; Tulli, D.; Baker, D.; Pruneri, V. Durable, Superhydrophobic, Antireflection, and Low Haze Glass Surfaces Using Scalable Metal Dewetting Nanostructuring. *Nano Res.* **2013**, *6* (6), 429–440.
- (30) Rombaut, J.; Fernandez, M.; Mazumder, P.; Pruneri, V. Nanostructured Hybrid-Material Transparent Surface with Antireflection Properties and a Facile Fabrication Process. *ACS Omega* **2019**, *4* (22), 19840–19846.
- (31) Barthlott, W.; Neinhuis, C. Purity of the Sacred Lotus, or Escape from Contamination in Biological Surfaces. *Planta* **1997**, *202* (1), 1–8.
- (32) Ensikat, H. J.; Ditsche-Kuru, P.; Neinhuis, C.; Barthlott, W. Superhydrophobicity in Perfection: The Outstanding Properties of the Lotus Leaf. *Beilstein J. Nanotechnol.* **2011**, *2* (1), 152–161.
- (33) Gao, L.; McCarthy, T. J. The “Lotus Effect” Explained: Two Reasons Why Two Length Scales of Topography Are Important. *Langmuir* **2006**, *22* (7), 2966–2967.
- (34) Bhushan, B.; Nosonovsky, M. The Rose Petal Effect and the Modes of Superhydrophobicity. *Philos. Trans. R. Soc., A* **2010**, *368* (1929), 4713–4728.
- (35) Chen, F.; Zhang, D.; Yang, Q.; Wang, X.; Dai, B.; Li, X.; Hao, X.; Ding, Y.; Si, J.; Hou, X. Anisotropic Wetting on Microstrips Surface Fabricated by Femtosecond Laser. *Langmuir* **2011**, *27* (1), 359–365.
- (36) Rombaut, J.; Maniyara, R. A.; Bellman, R. A.; Acquard, D. F.; Baca, A. S.; Osmond, J.; Senaratne, W.; Quesada, M. A.; Baker, D.; Mazumder, P.; Pruneri, V. Antireflective Transparent Oleophobic Surfaces by Noninteracting Cavities. *ACS Appl. Mater. Interfaces* **2018**, *10*, 43230–43235.
- (37) Peng, J.; Zhao, X.; Wang, W.; Gong, X. Durable Self-Cleaning Surfaces with Superhydrophobic and Highly Oleophobic Properties. *Langmuir* **2019**, DOI: 10.1021/acs.langmuir.9b01507.
- (38) Zhang, K.; Li, Z.; Maxey, M.; Chen, S.; Karniadakis, G. E. Self-Cleaning of Hydrophobic Rough Surfaces by Coalescence-Induced Wetting Transition. *Langmuir* **2019**, *35* (6), 2431–2442.
- (39) Mazumder, P.; Jiang, Y.; Baker, D.; Carrilero, A.; Tulli, D.; Infante, D.; Hunt, A. T.; Pruneri, V. Superomniphobic, Transparent, and Antireflection Surfaces Based on Hierarchical Nanostructures. *Nano Lett.* **2014**, *14*, 4677–4681.
- (40) Thompson, C. V. Solid-State Dewetting of Thin Films. *Annu. Rev. Mater. Res.* **2012**, *42*, 399–434.